

Iron partitioning in natural lower-mantle minerals: Toward a chemically heterogeneous lower mantle

FELIX V. KAMINSKY^{1,*} AND JUNG-FU LIN²

¹KM Diamond Exploration Ltd., West Vancouver, British Columbia V7S 3J1, Canada

²Department of Geological Sciences, Jackson School of Geoscience, The University of Texas at Austin, Austin, Texas, U.S.A.

ABSTRACT

The concentrations of Fe, Al, and Ni and their distributions were determined for all known natural assemblages of ferropericlase (fPer) and bridgmanite (Bridg), coexisting as inclusions in deep-mantle diamonds from Brazil, Canada, Guinea, and South Australia. Based upon these data, it is likely that some areas within the deep lower mantle are iron-rich and differ markedly from a pyrolitic composition. In the lowermost lower mantle, Bridg is Al-rich and fPer is Ni-poor, witnessing the presence of a free metallic phase in the mineral-forming environment. The iron partitioning in the Bridg + fPer association [$K_B^{\text{Bridg-fPer}} = ([\text{Fe}/\text{Mg}]^{\text{Bridg}})/([\text{Fe}/\text{Mg}]^{\text{fPer}})_{\text{at}}$] in juvenile diamond inclusions is as low as 0.1–0.2. During ascent of the diamonds with their inclusions to the surface, the $K_B^{\text{Bridg-fPer}}$ eventually increases to values of 0.4–0.5 and even as high as 0.7.

The details of the element partitioning between natural Bridg and fPer in the lower mantle are as follows: iron in Bridg is ferrous Fe^{2+} in the A site, substituting for Mg^{2+} ; almost all iron in fPer is ferrous Fe^{2+} ; the share of ferric Fe^{3+} iron in fPer is $\text{Fe}^{3+}/\Sigma\text{Fe} = 8\text{--}12$ at%; iron concentrations in both Bridg and fPer increase with depth (pressure), reflecting the increasing Fe content in the lower part of the lower mantle, different from that of a pyrolitic model. Al in Bridg is mainly in the cation site B and partly in the cation site A, in both cases substituting for Si, Mg, and Fe with vacancy formation; and in the case of Al positioning into both B and A sites, a charge-balanced reaction occurs.

The natural samples show very diverse $K_B^{\text{Bridg-fPer}}$ values and elemental distribution that cannot be simply explained by our current understanding on alumina dissolution in Bridg and the spin transition of Fe^{2+} in fPer. These major differences between experimental results and observations in natural samples demonstrate the complex, inhomogeneous iron speciation and chemistry in the lower mantle.

Keywords: Lower mantle, ferropericlase, bridgmanite, iron partitioning, pyrolite

INTRODUCTION

The Earth's lower mantle, based on a pyrolite compositional model, is believed to comprise three major mineral species, bridgmanite $[(\text{Mg,Fe})(\text{Si,Al})\text{O}_3]$, ferropericlase $[(\text{Mg,Fe})\text{O}]$, and calcium silicate perovskite $[\text{CaSiO}_3]$, that are gravitationally compressed near adiabatically. It has been proposed that these minerals are distributed homogeneously and have constant compositions, for the most part through the lower mantle, and thus contribute to continuous features of the observed, one-dimensional seismic model of density, compressional wave velocity and shear wave velocity (Dziewonski and Anderson 1981; Kennett et al. 1995). Bridgmanite (Bridg) and ferropericlase (fPer) contain significant amounts of iron, whose complex chemical speciation and electronic spin transitions can affect a broad spectrum of the physical and chemical properties of the two major phases of the lower mantle (e.g., Irifune et al. 2010; Lin et al. 2013).

High P - T experiments along an expected mantle geotherm for a pyrolitic composition demonstrated that the iron index, $f_e = \text{Fe}/(\text{Fe}+\text{Mg})_{\text{at}}$, of the pyrolitic lower-mantle fPer should be 0.12–0.27 (e.g., Wood 2000; Lee et al. 2004) or even lower, at ~0.10 (Kesson and Fitz Gerald 1991). These results suggest that the iron

chemistry of lower-mantle fPer may not vary significantly. However, although a majority of the studied natural lower-mantle fPer grains hosted within deep-diamond inclusions have $f_e = 0.10\text{--}0.20$, more than 40% of them vary in a “forbidden” range with up to $f_e = 0.62$, falling into the field of magnesiowüstite (e.g., Hutchison 1997; Kaminsky 2012); one of the analyzed samples has an iron index even as high as 0.9, which is almost close to the end-member wüstite stoichiometry. Some Bridg grains, coexisting with iron-rich fPer, also exhibit relatively high iron contents. The discovery of these iron-rich ferropericlase and magnesiowüstite grains deviates from the traditional view of the pyrolitic lower mantle composition that displays a homogenous iron chemistry and mineralogy, and points to a much more complex chemistry of the lower mantle.

To elucidate the lower-mantle chemistry in these minerals, we have analyzed Fe, Ni, and Al contents and their distribution in all the currently known fPer+Bridg assemblages coexisting as inclusions in natural diamonds from Brazil, Canada, Guinea, and South Australia.

REVIEW OF EXPERIMENTAL DATA

Several experimental works on iron partitioning between Bridg and fPer in a laser-heated diamond-anvil cell, subjected to relevant lower-mantle conditions of up to approximately 120 GPa, were performed over the last two decades. Almost all experiments modeled the suggested pyrolitic model of the lower mantle with

* E-mail: felixvkaminsky@aol.com

the iron index, $fe = \text{Fe}/(\text{Fe}+\text{Mg})_{\text{at}} = 0.05\text{--}0.10$. The only exception was the work performed by Tange et al. (2009) in a multi-anvil apparatus with sintered diamond anvils, in which the starting material was very different from pyrolitic and had $fe = 0.50$; it resulted in highly iron-rich association, Bridg with $fe = 0.16\text{--}0.32$ and fPer with $fe = 0.49\text{--}0.92$. The other studies have shown disparate results for the distribution of Fe in the various minerals (Fig. 1a). For example, while some demonstrated a positive correlation of the iron index between Bridg and fPer (0.070–0.234) (Katsura and Ito 1996; Kesson et al. 2002; Kobayashi et al. 2005; Murakami et al. 2005; Sakai et al. 2009); others found the opposite, a negative correlation (Irfune 1994; Kesson et al. 1998; Wood 2000; Irfune et al. 2010) (Fig. 1a). At $fe_{\text{fPer}} = 0.05\text{--}0.20$ for both trends, the positive correlation was obtained mainly in association with low-Fe Bridg ($fe = 0.010\text{--}0.103$), while the negative correlation was in association with high-Fe Bridg ($fe = 0.081\text{--}0.167$). There were, as well, experimental results showing variations in $fe_{\text{Bridg}} = 0.011\text{--}0.077$ virtually independently of fe_{fPer} (ca. 0.10) (Auzende et al. 2008). The general trends (I and II) can be identified in a consolidated graph (Fig. 1a). The positive trend divides into two branches (trends Ia and Ib) with the same correlation but different values of fe_{Bridg} which could be due to different pressure range examined. These experimental discrepancies remain unexplained.

Experimental evaluations of the partition coefficient of iron between fPer and Bridg defined as $K_{\text{D}}^{\text{Bridg-fPer}} = ([\text{Fe}/\text{Mg}]^{\text{Bridg}})/([\text{Fe}/\text{Mg}]^{\text{fPer}})_{\text{at}}$ produce even more inconsistent results. The values of $K_{\text{D}}^{\text{Bridg-fPer}}$ vary from 0.04 to 0.9 (Fig. 1b). Some of the experiments have shown an increase of $K_{\text{D}}^{\text{Bridg-fPer}}$ with pressure (Irfune 1994; Kobayashi et al. 2005; Sinmyo and Hirose 2013), whereas others have demonstrated the reverse (Andrault 2001; Kesson et al. 2002; Murakami et al. 2005; Tange et al. 2009; Irfune et al. 2010), or have found no correlation between $K_{\text{D}}^{\text{Bridg-fPer}}$ and pres-

sure (Guyot et al. 1988; Katsura and Ito 1996; Auzende et al. 2008). Specifically, the concentration of Al^{3+} in bridgmanite has been shown to significantly affect its iron partitioning and Fe^{3+} content; it has been shown that the dissolution of Al^{3+} in bridgmanite at the top lower-mantle conditions can significantly enhance the Fe^{3+} occupancy in the A site of the lattice resulting in higher $K_{\text{D}}^{\text{Bridg-fPer}}$ (Irfune et al. 2010). The cause of these discrepancies may relate to dissimilar conditions under which the experiments were performed (great thermal gradients, pressure duration, chemical homogeneity, non-thermodynamic equilibrium, etc.) and/or in the compositions of starting materials, including different concentrations of Fe and Al used in the experiments.

The discovery of iron spin crossover in fPer led to the suggestion that $K_{\text{D}}^{\text{Bridg-fPer}}$ would behave differently in relevant high P - T conditions found in the deep lower mantle, decreasing from the mid-lower mantle to bottom lower mantle conditions, such that most of the iron partitions into fPer leaving Bridg essentially iron-free (Badro et al. 2003; Speziale et al. 2005). More recent theoretical and experimental studies on a pyrolite composition have found that $K_{\text{D}}^{\text{Bridg-fPer}}$ increases from approximately 0.5 at top-lower mantle conditions to 0.8–0.9, at about 800 km in depth due to the suggested coupled substitution of Al^{3+} and Fe^{3+} in Bridg, but then decreases to 0.4 or even lower due to the spin crossover of iron in fPer at mid-lower mantle conditions (Wood and Rubie 1996; Irfune et al. 2010; Vilella et al. 2015; Xu et al. 2017). However, a high P - T diamond-anvil cell study, using a pyrolite composition, has shown that $K_{\text{D}}^{\text{Bridg-fPer}}$ increases to 0.9 at bottom-lower mantle conditions, suggested to be due to the spin transition of Fe^{3+} in Bridg (Sinmyo and Hirose 2013). Recently, Fe-bearing bridgmanite has been reported to dissociate into Fe-rich phase, called H-phase, and MgSiO_3 -rich bridgmanite at deep lower mantle P - T conditions (Zhang et al. 2014), which can challenge the aforementioned conventional view of the iron index in the lower-mantle mineral assemblage. However, this report remains to be verified experimentally and theoretically. Thus far, a consensus on the iron partition coefficient across the spin transition in the lower-mantle assemblage has not yet been reached, especially under natural compositional, oxygen fugacity, and P - T environments.

RESULTS

To date, several Bridg, fPer, and other lower-mantle minerals have been identified as natural inclusions in diamonds collected from Brazil, Canada, Guinea, Australia, and some other countries, and subsequently analyzed (Kaminsky 2012 and references therein). The details of these finds and analytical procedures are presented elsewhere, including references to Tables 1 and 2 and Supplementary¹ Table 1. Among them, are 19 Bridg + fPer pairs, each of which coexist in the same diamond, sometimes in a close (“touching”) association, i.e., formed under equilibrium conditions. This relationship permits studies of the distribution and partitioning of iron and other elements within the media where those minerals originated within the lower mantle (Supplementary¹ Table 1). We should note that the Bridg samples in these assemblages may have retrograde transformation into enstatite under ambient conditions, but several physical and chemical characteristics established in previous studies justified their deep lower mantle origin as Bridg (e.g., Harte et al. 1999; Kaminsky 2012; Tschauner et al. 2014).

Ferropericlase

Ferropericlase in the lower-mantle compositional model has been typically assumed to exhibit a composition with $fe = 0.08\text{--}0.11$ and even more precisely, at ~ 0.10 (Kesson and Fitz Gerald 1991). In the natural environment, however, fPer may be much more iron-rich, up to $fe = 0.64$, and sometimes even up to 0.90; as such, this does not correspond to the pyrolitic composition of the formation media. Recently, Fe-rich magnesiowüstite

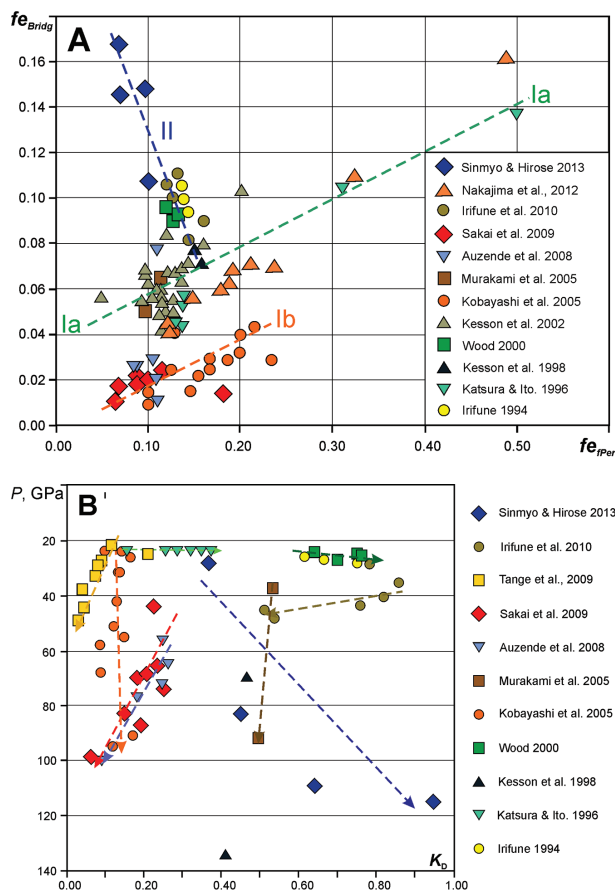


FIGURE 1. Summary of literature experimental results of iron partitioning between bridgmanite and ferropericlase at high pressures and temperatures. (a) fe_{Bridg} vs. fe_{fPer} in all experiments performed to date. I and II show general trends. (b) Partition coefficient $K_{\text{D}}^{\text{Bridg-fPer}}$ under different pressure values. (Color online.)

¹Deposit item AM-17-45949, Supplemental Table 1. Deposit items are free to all readers and found on the MSA web site, via the specific issue's Table of Contents (go to http://www.minsocam.org/MSA/AmMin/TOC/2017/Apr2017_data/Apr2017_data.html).

has been observed to occur in melting of subducted slabs in the mantle at approximately 300–700 km in depth (Thomson et al. 2016), providing a mechanism for the formation of very Fe-rich fPer in the lower mantle. TEM studies with the use of EDX and EEL spectroscopy demonstrated that ferric iron in fPer grains is located in exsolved non-stoichiometric Fe³⁺-enriched clusters (Mg_{1-x}Fe_{2-x}O_{4-x/2}), varying in size from 1–2 to 10–15 nm and comprising ~3.6 vol% of fPer, while the remaining iron in fPer is in the ferrous, Fe²⁺ state (Fig. 2a) (Kaminsky et al. 2015a). Recent work by Nestola et al. (2016) demonstrated a possibility for studying the internal structure of ferropericlae and distribution of ferric iron in it (including its exsolved phases) with the use of in situ synchrotron Mössbauer spectroscopy. As the host

diamond ascended through the uppermost lower mantle, these iron-rich clusters experience falling pressure conditions that resulted in their release and formation of 10–50 nm sized magnesianiferite MgFe₂O₄ crystals, developing along dislocations in fPer with a precise orientation relationship between both phases: (022)_{mFer}//(022)_{fPer}; (11 $\bar{1}$)_{mFer}//(11 $\bar{1}$)_{fPer} and the zone axis for both phases is [2 $\bar{1}$ 1] (Fig. 2b) (Kaminsky et al. 2015b).

Bridgmanite

Bridgmanite is a member of the perovskite family with an orthorhombic distortion of the ideal cubic perovskite structure and a general formula, ^{VIII/XII}A²⁺^{VI}B⁴⁺O₃²⁻ (where VI, VIII, and XII are cation fold positions), in which A larger (mainly divalent)

TABLE 1. Cation fractions of natural lower-mantle bridgmanite (in atomic numbers)

Sample no.	Mg	Fe	Ni	Mn	Ca	Na	K	A _{total} (VIII/XII)	Si	Al	Ti	Cr	B _{total} (VI)	Refs ^a
Juina area, Brazil														
BZ120	0.878	0.064	0.000	0.002	0.001	0.002	0.000	0.948	0.943	0.024	0.003	0.006	0.976	1
BZ207	0.795	0.125	0.000	0.004	0.001	0.002	0.000	0.928	0.923	0.052	0.003	0.002	0.980	1
BZ210	0.750	0.071	0.000	0.013	0.012	0.034	0.006	0.885	0.856	0.197	0.000	0.016	1.069	1
BZ241	0.674	0.075	0.000	0.018	0.012	0.027	0.000	0.805	0.903	0.201	0.000	0.015	1.120	1
BZ242	0.406	0.055	0.000	0.018	0.078	0.149	0.000	0.707	0.915	0.247	0.000	0.023	1.185	1
BZ251	0.900	0.053	0.000	0.002	0.001	0.001	0.000	0.957	0.950	0.026	0.002	0.005	0.983	1
14-2	0.833	0.068	0.000	0.002	0.021	0.004	0.000	0.928	0.946	0.027	0.001	0.006	0.980	2
1-5	0.863	0.087	0.000	0.002	0.001	0.000	0.000	0.953	0.934	0.041	0.001	0.003	0.979	3
3-2	0.830	0.059	0.000	0.002	0.001	0.000	0.000	0.891	0.969	0.031	0.003	0.003	1.006	3
3-5	0.824	0.092	0.000	0.004	0.000	0.000	0.000	0.920	0.927	0.061	0.003	0.003	0.993	3
4-3	0.877	0.059	0.000	0.001	0.000	0.002	0.000	0.941	0.933	0.048	0.003	0.004	0.987	3
Northwest Territories, Canada														
DO2700100	0.940	0.040	0.000	0.001	0.007	0.000	0.000	0.988	0.956	0.014	0.000	0.004	0.973	4
DO2700300	0.938	0.041	0.000	0.001	0.001	0.002	0.000	0.984	0.981	0.014	0.000	0.004	0.998	4
DO27-97 14A	0.896	0.059	0.000	0.001	0.002	0.001	0.000	0.959	0.953	0.040	0.000	0.005	0.998	4
Kankan area, Guinea														
KK-103	0.891	0.047	0.000	0.001	0.001	0.001	0.000	0.942	0.955	0.012	0.000	0.002	0.970	5
KK-108	0.866	0.068	0.000	0.002	0.002	0.001	0.000	0.939	0.946	0.033	0.001	0.003	0.983	5
KK-16	0.892	0.046	0.000	0.002	0.001	0.002	0.000	0.943	0.957	0.011	0.000	0.004	0.972	5
KK-44	0.911	0.049	0.000	0.002	0.001	0.002	0.000	0.965	0.962	0.023	0.001	0.005	0.991	5
Eurelia area, South Australia														
FBS5-11	0.908	0.041	0.001	0.002	0.001	0.000	0.000	0.953	0.999	0.005	0.000	0.005	1.010	6

Notes: A_{total} and B_{total} represent the total cation fraction in the A and B site, respectively. ^a References: 1 = Hutchison (1997), 2 = Zedgenizov et al. (2014), 3 = Hayman et al. (2005), 4 = Davies et al. (2004), 5 = Stachel et al. (2000), 6 = Tappert et al. (2009).

TABLE 2. Compositions of coexisting bridgmanite and ferropericlae included in the lower-mantle diamonds

Sample no.	Mineral association	Bridgmanite				Ferropericlae				K _{fPer} ^{Bridg}	Refs ^a
		FeO (wt%)	MgO (wt%)	Al ₂ O ₃ (wt%)	fe	FeO (wt%)	MgO (wt%)	Ni (ppm)	fe		
Juina area, Brazil											
BZ120	Bridg+fPer	4.63	35.39	1.23	0.069	42.81	55.25	6052	0.310	0.1688	1
BZ207	Bridg+fPer+Jeffbenite	9.02	32.03	2.66	0.138	43.14	54.84	7074	0.313	0.3580	1
BZ210	Bridg+fPer	5.14	30.21	10.04	0.088	27.20	69.22	9982	0.183	0.4330	1
BZ241	Bridg+fPer+Ruby	5.36	27.15	10.24	0.101	28.63	68.21	11711	0.193	0.4704	1
BZ242	Bridg+fPer	3.95	16.35	12.58	0.120	25.50	69.30	11083	0.173	0.6566	1
BZ251	Bridg+fPer	3.80	36.25	1.33	0.056	23.52	74.77	9825	0.152	0.3332	1
14-2	Bridg+fPer+Di?	4.87	33.59	1.37	0.086	31.50	65.60	9746	0.216	0.3019	2
1-5	Bridg+fPer	6.25	34.80	2.07	0.093	36.70	60.98	9137	0.258	0.2982	3
3-2	Bridg+fPer+CaSiPv+'Ol'	4.21	33.43	1.60	0.066	25.27	72.21	10336	0.166	0.3599	3
3-5	Bridg+fPer+'Ol'	6.60	33.20	3.10	0.101	48.96	50.34	2437	0.363	0.2044	3
4-3	Bridg+fPer+'Ol'	4.27	35.36	2.45	0.064	25.67	71.11	10631	0.168	0.3810	3
Northwest Territories, Canada											
DO2700100	Bridg+fPer+CaSiPv+SiMg	2.85	37.90	0.69	0.041	16.80	81.60	8882	0.104	0.3652	4
DO2700300	Bridg+fPer+'Ol'	2.97	37.80	0.72	0.042	23.60	73.70	11083	0.154	0.2454	4
DO27-97 14A	Bridg+fPer+Ni	4.22	36.11	2.03	0.062	21.29	77.45	10742	0.135	0.4251	4
Kankan area, Guinea											
KK-103	Bridg+fPer	3.39	35.92	0.61	0.050	20.11	76.98	11004	0.129	0.3876	5
KK-108	Bridg+fPer+Ga	4.90	34.90	1.67	0.037	22.15	75.61	10049	0.143	0.4788	5
KK-16	Bridg+fPer+Siderite	3.34	35.94	0.55	0.050	22.68	75.34	11212	0.146	0.3425	5
KK-44	Bridg+fPer+CaSiPv+'Ol'	3.52	36.73	1.19	0.051	20.15	76.45	10532	0.130	0.3634	5
Eurelia area, South Australia											
FBS5-11	Bridg+fPer	2.93	36.58	0.25	0.043	23.42	74.04	9550	0.152	0.2532	6

Notes: Bridg = bridgmanite; fPer = ferropericlae; Di? = suggested diopside; CaSiPv = CaSi-perovskite; 'Ol' = phase with an olivine composition; SiMg = unidentified Si-Mg phase; Ni = native Ni; Ga = garnet.

^a Reference numbers are the same as in Table 1.

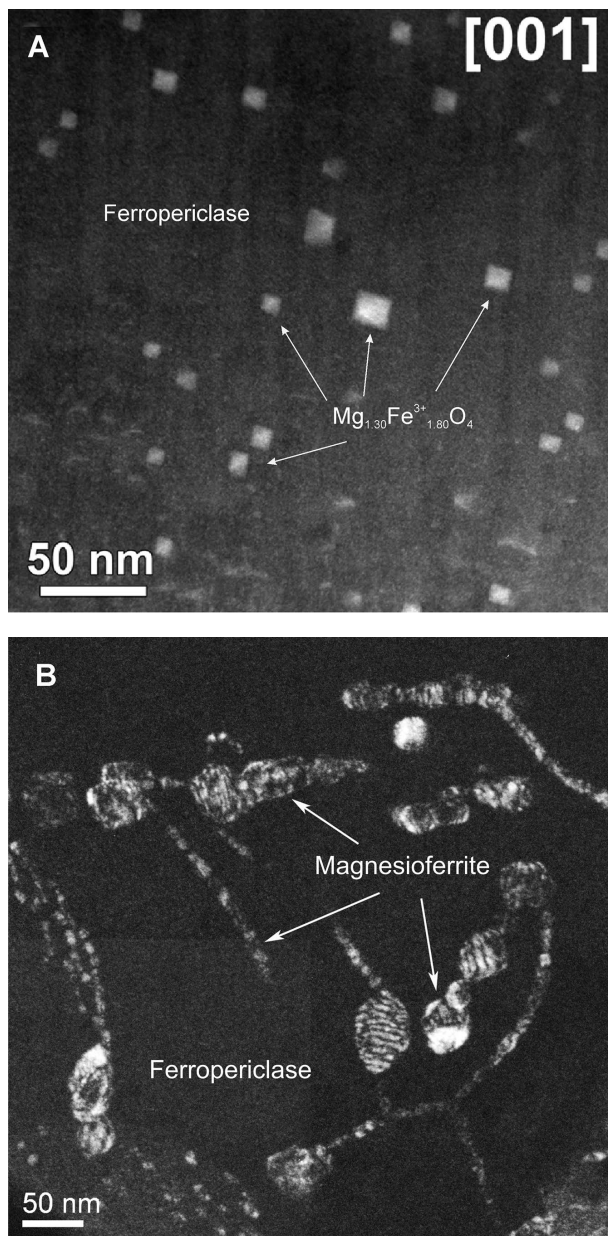


FIGURE 2. Exsolution of Fe^{3+} -rich phases in ferropericlyase. (a) $\text{Mg}_{1.30}\text{Fe}_{1.80}\text{O}_4$ truncated octahedra (bright) in a ferropericlyase dark matrix; high-angle annular dark-field scanning transmission electron-microscopy image by A. Abakumov (Kaminsky et al. 2015a). (b) Magnesioferrite, $\text{MgFe}_2^+\text{O}_4$, octahedral and cubic grains, developed along dislocations in ferropericlyase. Dark-field TEM image by R. Wirth (Kaminsky et al. 2015b).

pseudo-dodecahedral (8/12-fold) site cations mostly include Mg, Fe^{2+} , Mn, Ni, Ca, and some other elements, and B smaller sixfold-site cations are Si, Al, and partly Fe^{3+} . The analyzed natural lower-mantle bridgmanite samples have cation compositions as presented in Table 1.

Most of the grains have compositions close to stoichiometric Bridg. Some deficit in both cation groups is likely caused by the presence of other, non-analyzed cations, such as P and REE,

which are characteristic for this group of minerals. Judging by crystal-chemical calculations (Table 1), all iron substitutes for Fe^{2+} in the A site and, most likely, is in the divalent form, Fe^{2+} , although McCammon et al. (1997), based on Mössbauer spectroscopy, suggested a significant portion of iron to be Fe^{3+} . There is no evidence for the presence of Fe^{3+} in the B site in natural Bridg. The three most Al-rich specimens (BZ210, BZ241, and BZ242, all from Brazil) show excess in alumina in the amounts of 0.069–0.185. These amounts balance the deficit in cation site A of these specimens, implying the location of this portion of Al to be in the 8/12-fold pseudo-octahedral coordination position.

Partition coefficient of iron in natural bridgmanite+ferropericlyase assemblages

The analysis of the iron index fe in coexisting fPer and Bridg grains and the partition coefficient of iron $K_D^{\text{Bridg-fPer}}$ in all Bridg+fPer assemblages shows that two groups of assemblages can be distinguished (Table 2; Fig. 3a). The first group (Group A; 84% of all pairs) forms an elongated cloud illustrating a general positive correlation between $fe_{\text{Bridg}} = 0.032\text{--}0.138$ and $fe_{\text{fPer}} = 0.116\text{--}0.363$. The correlation trend is close to trend Ia from the experimental data, confirming the regularity in Fe exchange between the two major lower-mantle minerals. The second group (Group B; 16% of all grains) is composed of three specimens with almost constant $fe_{\text{fPer}} = 0.173\text{--}0.193$ and relatively high fe_{Bridg} , varying from 0.088 to 0.120; all specimens are high-Al varieties. This group lies outside of any experimental trends. The increase in fe of both natural fPer and Bridg from Group A is independent of the $K_D^{\text{Bridg-fPer}}$ values (0.169–0.479), while Group B, which has fe values in the same range as Group A, has elevated values of $K_D^{\text{Bridg-fPer}} = 0.433\text{--}0.657$ (Fig. 3b).

Such variations in the iron indices and the bulk iron contents in the coexisting, major lower-mantle minerals differs drastically from what was expected for a pyrolytic lower mantle with a homogeneous distribution of iron in fPer and Bridg (Kesson and Fitz Gerald 1991; Wood 2000; Lee et al. 2004). According to the experimental and theoretical data for a bulk pyrolytic composition, where the total iron content in the system was fixed at $fe = 0.09\text{--}0.15$ (Irifune et al. 2010; Vilella et al. 2015; Xu et al. 2017), we should expect a decrease of the iron content in Bridg with an increase of the iron content in fPer. In reality, it is not the case, however, as both fPer and Bridg demonstrate the simultaneous, well-correlated increase of fe values (Figs. 3a–d).

Both groups of assemblages are characterized by similar concentrations of Ni in fPer, mainly corresponding to the bulk Ni contents in the mantle (6052–11 212 ppm from Group A and 9982–11 711 ppm from Group B) (Fig. 3c). However, one of the analyzed samples (no. 3–5 from Brazil) has a low concentration of Ni = 2437 ppm, and there are several low-Ni fPer inclusions in diamond (Fig. 4a). Analysis of the Ni content in fPer as a function of the iron index shows that the fPer grains with fe of approximately 0.2 in deep-diamond inclusions (circled in Fig. 4b) have Ni contents close to the estimates of 8000–12 000 ppm for the bulk pyrolytic composition; however, the Ni content drastically decreases with increasing iron index in fPer, especially for samples from Brazil (Fig. 3b). The samples with fe of more than 0.6 from Brazil have Ni contents less than 2000 ppm. So, the analyses of natural fPer grains show that the higher the iron

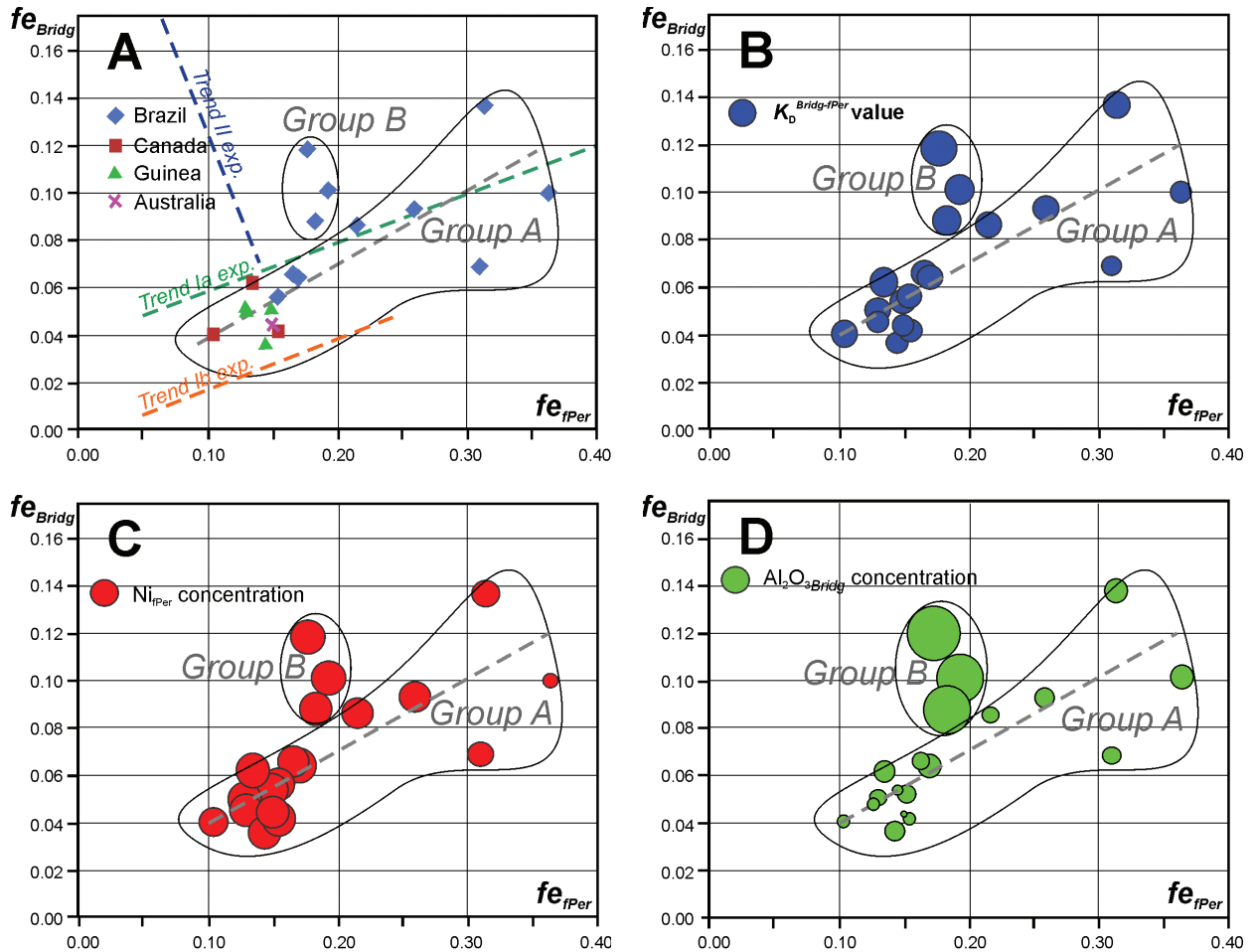


FIGURE 3. Iron indices $fe = \text{Fe}/(\text{Fe}+\text{Mg})_{\text{at}}$ in coexisting natural ferropericlase and bridgmanite in lower-mantle diamond inclusions. (a) General plot. (b) With $K_D^{\text{Bridg-fPer}}$ values, shown as circles, the radii of which are proportional to the $K_D^{\text{Bridg-fPer}}$ values. (c) With Ni concentrations in ferropericlase, shown as circles, the radii of which are proportional to the Ni concentrations. (d) With Al_2O_3 concentrations in bridgmanite, shown as circles, the radii of which are proportional to the Al_2O_3 concentrations. Four groups of samples from Brazil, Canada, Guinea, and Australia with the fPer and Bridg grains that associate with each other are used. (Color online.)

index in the grain, the lower the Ni content.

There is a general (although not very strong) positive correlation between Ni and the partition coefficient of iron (Fig. 4a). The lowest $K_D^{\text{Bridg-fPer}}$ values (0.169 in sample numbers BZ120 and 0.204 in sample no. 3–5) are characterized by the lowest Ni concentrations in fPer, whereas the samples with the highest $K_D^{\text{Bridg-fPer}}$ values (nos. BZ210, BZ241n, and BZ242) are characterized with the highest Ni contents in fPer.

DISCUSSION

Role of Ni and Al in the iron partition coefficient distribution

The Ni concentration in fPer indicates the presence of metallic iron phase(s) in the magmatic system of the deep mantle, as established by Frost et al. (2004). It was shown that the increasing weight fraction of metallic phase (suggesting the conditions present within the lowermost lower mantle) leads to a decrease of Ni concentration in the lower-mantle material and also to a decrease of the concentration of this element in coexisting fPer

and Bridg (Ryabchikov and Kaminsky 2013). In this process, iron acts as a dilutant of Ni dissolved in metal. According to experimental data (Frost et al. 2004; Frost and McCammon 2008), metal content in the lower mantle is estimated at 1 wt% (10000 ppm) before the release of metallic alloy. This implies that the fPer grains with high Ni concentrations were formed in media that did not contain metallic alloy (or its quantity was extremely small), suggesting these originated within the uppermost lower mantle, while the low Ni fPer grains were formed in the presence of metallic alloy within lower parts of the lower mantle. More than 40% of the studied lower-mantle fPer grains are low-Ni and high-Fe inclusions. These variations in Fe and Ni concentrations in fPer point to a radial compositional gradient in the lower mantle at the time of the formation of these minerals, and the anti-correlation of Ni and Fe in fPer may be applied as a qualitative criterion of the depth of its origin.

The correlation between the $K_D^{\text{Bridg-fPer}}$ values and Ni concentrations in fPer (Fig. 4a) is not strong because of the presence of other elements in minerals, such as Al, Co, Mn, Na, etc. The

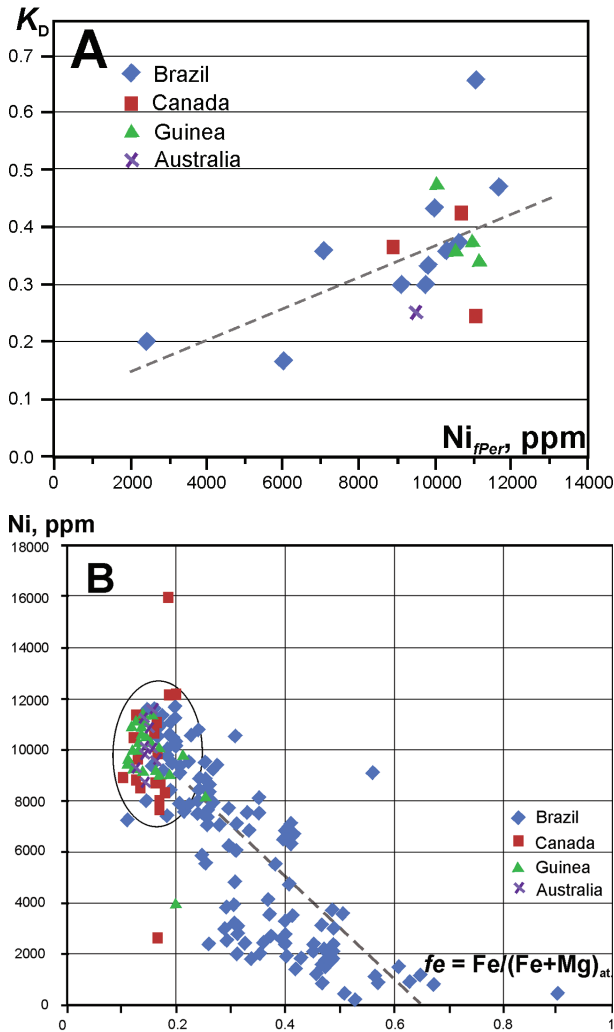


FIGURE 4. Variations of Ni concentrations in natural ferropericlaise. (a) $K_D^{Bridg-Per}$ vs. Ni content in ferropericlaise. (b) Ni content vs. iron index in all analyzed to date ferropericlaise grains entrapped by lower-mantle diamonds. Data from Kaminsky (2012) and references therein. (Color online.)

major factor here is the Al impurity in Bridg, which is the real cause for the existence of the two groups of associations (Fig. 3d). Al_2O_3 in Bridg comprises 0.69–3.10 wt% in Group A and 10.04–12.58 wt% in Group B. In general, $K_D^{Bridg-Per}$ correlates with the Al_2O_3 content in Bridg, which is particularly noticeable for the Brazilian samples (Fig. 5a). However, this correlation is quite weak (Figs. 5a and 5b) and requires further understanding.

The enrichment of Bridg with Al is strongly pressure dependent (Andrault et al. 2007). In the uppermost part of the lower mantle Al-rich phases, such as majorite and jeffbenite, still occur. In experiments at pressure conditions of 24–28 GPa these minerals dissociate, and the released Al is incorporated into Bridg (Irfune and Tsuchiya 2007). In the natural environment, the reverse scenario occurs: juvenile high-Al Bridg at 24–28 GPa releases Al with the formation of Al-bearing phases, such as majorite and jeffbenite (formerly known as TAPP; Nestola et al. 2015).

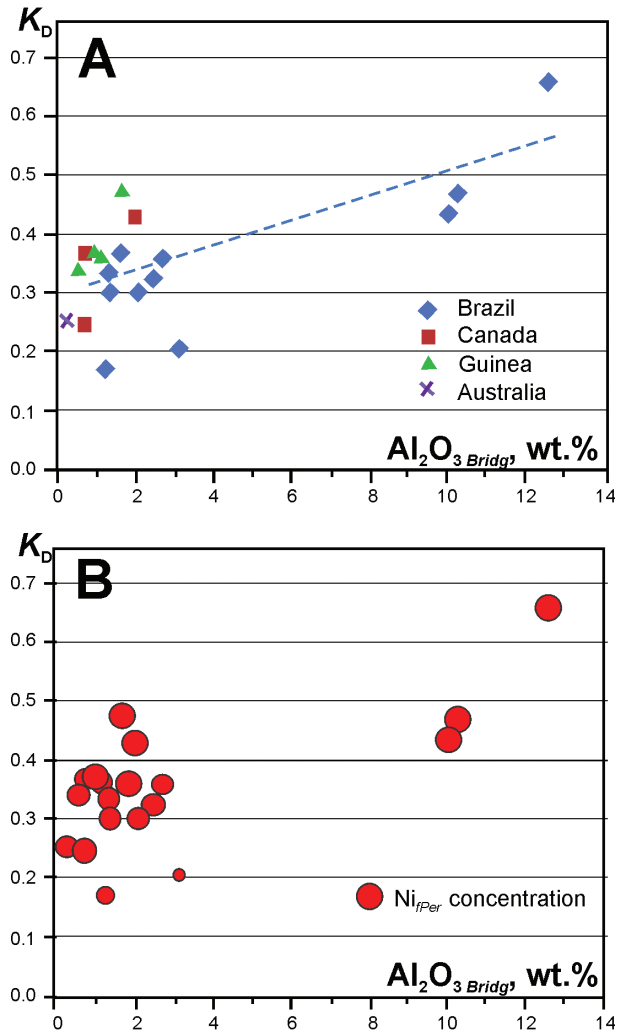
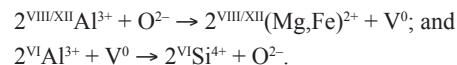
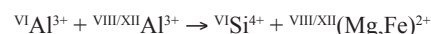


FIGURE 5. Iron partitioning coefficient $K_D^{Bridg-Per}$ vs. Al_2O_3 content in bridgmanite. (a) General plot. (b) With Ni concentrations in ferropericlaise from Brazil, Canada, Guinea, and Australia, shown as circles, the radii of which are proportional to the Ni contents. (Color online.)

As a result, the following scenario can be outlined for the lower mantle. Bridg has a high, up to 10–12 wt% concentration of Al_2O_3 , which is consistent with its bulk concentration in the primitive mantle of 4–5 mol% (e.g., McDonough and Sun 1995). Al occupies its position in both cation sites, A and B. In each case Al substitutes for Si and divalent cations with oxygen-vacancy formation as follows:



And in the case of Al positioning in both A and B sites, a charge-coupled mechanism, for which no oxygen vacancies are required for charge balance, takes place (Richmond and Brodholt 1998):



which, according to ab initio calculations, dominates at lower mantle pressures and temperatures (Akber-Knutson and Bukowski 2004). The concentration of Al in Bridg, particularly in the A site may indicate the depth of the mineral's origin, because previous studies have shown that Al concentration in Bridg increases with increasing pressure along a representative lower-mantle geotherm (Irifune et al. 2010). Recently an experimental study of the system $\text{MgSiO}_3\text{-Al}_2\text{O}_3$ under pressures up to 52 GPa and 2000 K, with the use of sintered diamond anvils combined with in situ synchrotron X-ray diffraction observations in a multi-anvil apparatus, demonstrated that the Al_2O_3 content in bridgmanite increases from 12 mol% at 27 GPa to 29 mol% at 52 GPa, suggesting that the Al_2O_3 content in bridgmanite can be used as a pressure indicator at pressures above 30 GPa (Liu et al. 2016).

As was shown above (Section 2, Table 1), iron in Bridg is in the A site, most likely in a ferrous divalent form. fPer with depth (and correspondingly increasing pressure) has a decreasing concentration of Ni and increasing f_e values, reflecting the increase in the iron content in the lower mantle. The decrease of Ni content in fPer may, therefore, be used as another qualitative geobarometer in the lower mantle.

In contrast to experimental conditions, most of which were performed with a pyrolitic compositions ($f_e = 0.05\text{--}0.15$), our results on natural samples show that iron indices in Bridg and fPer have positive correlation (Fig. 3), demonstrating the total enrichments of the lower-mantle media in iron. This enrichment is correlated with the Ni (negatively, Fig. 3c) and Al_2O_3 (positively, Fig. 3d) concentrations, each of which is an independent criterion of the increasing pressure. One may conclude that the Fe content of the lower mantle increases with depth and may differ from the pyrolitic composition. Iron in fPer is predominantly in a divalent form; the share of Fe^{3+} ions is $\text{Fe}^{3+}/\Sigma\text{Fe} = 8\text{--}12$ at% (Kaminsky et al. 2015a). Ferric iron in fPer grains is located in exsolved non-stoichiometric Fe^{3+} -enriched nanometer-sized clusters $\text{Mg}_{1+x}\text{Fe}_{2-3x}\text{O}_{4-x/2}$, while all remaining iron in fPer is in the ferrous, Fe^{2+} , state.

The discussion above opens new scenarios regarding the actual composition of the main minerals of the lower mantle, and the situation may be even more complex if we include additional phases that are present in the natural systems. Our interpretation of the new data on Fe, Ni, and Al distribution in Bridg and fPer explains the controversies in aforementioned high P - T experimental results of experiments, carried out in simplified closed systems.

Regional differences in the distribution of iron in ferropericlasite and bridgmanite

There are observed differences in the iron index of fPer values and related characteristics from different regions. For example, fPer from Canada, South Australia, and South Africa have $f_e = 0.10\text{--}0.20$ that are close to the pyrolite values. fPer from Guinea, along with similar f_e values, also has higher f_e values of 0.25. Moreover, iron-rich fPer from Brazil (reaching the composition of magnesiowüstite) comprises almost a half of all grains in this region (ca. 46.5%). It has been suggested that such differences represent different depths, at which the host diamonds sampled the lower mantle. In a pyrolitic lower

mantle, the average amount of iron in the lower-mantle minerals is commonly believed to be close to 10%, chiefly distributed between Bridg and fPer phases (Irifune et al. 2010). Here our analyses of the iron indices in these phases have shown that the total iron content in some of these minerals can be much higher than what is expected for a "normal" lower mantle. As shown in Figure 2, the occurrence of these "anomalous," high-Fe fPer and high-Fe Bridg pairs with $f_e = 0.17\text{--}0.36$ and $0.07\text{--}0.14$, respectively, indicates that the lower mantle is chemically inhomogeneous with respect to iron content at least in certain regions where these assemblages originated.

Recent high-resolution seismic tomography studies have revealed detailed seismic signatures of the lower mantle where strong seismic heterogeneities exist. Specifically, the Large Low Shear Velocity Provinces (LLSVPs) beneath the central Pacific and South Africa, extending from the core-mantle boundary up to approximately 1000 km above, exhibit reduced shear wave velocities and enhanced densities (e.g., Garnero and McNamara 2008). These regions are believed to contain dense, iron-rich piles that contribute to the "low shear velocity" and high density signatures in seismic observations; the iron enrichment in the regions may be due to core-mantle interaction, residuals of the magma ocean, and/or recycling of primordial materials, relative to the surrounding lower mantle (Garnero and McNamara 2008). On the other hand, thin patches of the Ultralow Velocity Zones (ULVZs), which are 5 to 40 km thick patches directly above the core-mantle boundary, exhibit reduced P - and S -wave velocities by up to 10 and 30%, respectively, and enhanced densities of up to 10% (Bower et al. 2011). These characteristics have been explained as a result of some partial melts and/or iron-enrichment in Bridg or silicate post-perovskite due to core-mantle reaction at the lowermost mantle (Garnero and McNamara 2008; Mao et al. 2010). We suggest that our analyzed Bridg+fPer pairs, which contain abnormally high iron indices, as shown in the second group in Figures 3b, 3c, and 3d, may originate from these regions that likely contain much higher amounts of iron than "normal" lower mantle regions.

Major differences in iron partitioning between natural samples and mineral physics results

In considering a natural system, we should expect the following scenario for depth, which should take into account the iron partitioning induced by the spin and valence transitions of iron ions proposed experimentally and theoretically, as well as significant iron chemistry heterogeneities at relevant P - T conditions of the lower mantle.

In the last decade, the discovery of a high-spin to low-spin crossover of Fe in the lower-mantle fPer and Bridg has been shown to influence their physical, chemical, rheological, and transport properties that can produce significant geophysical and geochemical consequences for our understanding of the deep Earth (e.g., Badro et al. 2003; Cammarano et al. 2010; Lin et al. 2013; Wu and Wentzcovitch 2014; Yang et al. 2015). The spin crossover of Fe^{2+} in fPer has been theoretically predicted to occur and experimentally observed at P - T conditions corresponding to the middle and the lower parts of the lower mantle (e.g., Tsuchiya et al. 2006; Lin et al. 2007); though, the spin transition of Fe^{3+} in magnesioferrite and its associated effects remain unknown. On the other hand, mineral physics studies of Bridg demonstrated

that Bridg can contain a very significant amount of Fe³⁺ in its lattice at the top lower mantle conditions, in which both Fe²⁺ and Fe³⁺ in the pseudo-dodecahedral site (A site) of the orthorhombic structure likely remain in the high-spin state at lower-mantle pressures, while a high-spin to low-spin transition of Fe³⁺ in the octahedral site (B site) occurs at pressures of 15–50 GPa (e.g., Hsu et al. 2012; Lin et al. 2013). Recent theoretical calculations considering a wide range of oxygen fugacity conditions and different iron spin and valence states, in the lower-mantle pyrolite assemblage, have further indicated that the Fe³⁺ content in Bridg decreases with increasing depth in the lower mantle; at lowermost lower mantle conditions, Fe³⁺ content in Bridg becomes almost negligible (Xu et al. 2017). Analyses of the natural Bridg and fPer assemblages show that most of the iron residing in the A site of Bridg lattice is in the Fe²⁺ state, which confirms these mineral physics studies.

High *P-T* experiments have further shown that the partition coefficient $K_D^{\text{Bridg-fPer}}$ is observed to increase from approximately 0.5 at 23 GPa up to 0.85 at about 28 GPa (~800 km in depth) and that can be associated with the Al³⁺-Fe³⁺ coupled substitution in Bridg in a pyrolytic composition, where iron ions partition almost equally between the fPer and Bridg lattices (Irifune et al. 2010). Results from such high *P-T* experiments showed that the $K_D^{\text{Bridg-fPer}}$ value stays almost constant at ~0.85 at pressures of between 28 and 40 GPa (~800–1000 km in depth) and then notably decreases to 0.4–0.5 with increasing pressures at 40–50 GPa (1000–1200 km in depth) (Irifune et al. 2010). This dramatic decrease is most likely associated with the spin transition of Fe²⁺ in fPer, which results in a volume collapse of about 2% (e.g., Lin et al. 2013) promoting iron ions in Bridg to favorably partition into the low-spin fPer which is energetically more stable than the high-spin Bridg and fPer. Without the alumina substitution in Bridg at such conditions, the $K_D^{\text{Bridg-fPer}}$ values decrease to approximately 0.2 (e.g., Sakai et al. 2009), i.e., lower than the value suggested from high *P-T* experiments using a pyrolytic composition (Irifune et al. 2010). That is, in an alumina-poor environment in the lower mantle, such as the olivine-rich peridotite environment, the $K_D^{\text{Bridg-fPer}}$ value is expected to remain low at approximately 0.2 with or without the spin transition effect. If the lower mantle is chemically pyrolytic, these changes in the iron partitioning indicate that the deeper parts of the lower mantle, especially toward the lowermost parts would likely contain iron-enriched, low-spin fPer and iron-poor, alumina-rich Bridg, whereas in the upper parts of the lower mantle, especially at approximately 800 km in depth, iron would almost equally partition between Bridg and fPer (Irifune et al. 2010). Comparison of these experimental results with our analyses on natural samples, however, clearly shows contradictory $K_D^{\text{Bridg-fPer}}$ values; the natural samples show very diverse $K_D^{\text{Bridg-fPer}}$ values that cannot be simply explained by the alumina dissolution in Bridg and the spin transition of Fe²⁺ in fPer. These major differences in the iron indices and $K_D^{\text{Bridg-fPer}}$ values demonstrate the complex, inhomogeneous iron speciation and chemistry in the lower mantle that are well beyond the knowledge of current mineral physics studies.

IMPLICATIONS

We conclude that some areas in the deep lower mantle are iron-rich and differ markedly from a pyrolytic composition, im-

plying that the bulk composition of the Earth is non-chondritic. The juvenile iron partitioning in the Bridg + fPer association ($K_D^{\text{Bridg-fPer}}$) is as low as 0.1–0.2. During the crystallization of diamonds at relatively shallower depth of the lower mantle, in which $K_D^{\text{Bridg-fPer}}$ increases to 0.4–0.5 and even as high as 0.7, they sample and deliver to the surface such associations. This regularity, established on geological samples, was supported by recently published theoretical calculations by Muir and Brodholt (2016), showing a decrease of $K_D^{\text{Bridg-fPer}}$ with depth from 0.32 to 0.06.

The details of the element partitioning between natural Bridg and fPer, in the lower mantle (at least in some areas), are as follows:

- According to crystal-chemical calculations, iron in Bridg is ferrous, Fe²⁺, in the A site, substituting for Mg²⁺;
- Almost all iron in fPer is ferrous Fe²⁺; the share of ferric, Fe³⁺, iron in fPer is Fe³⁺/ΣFe = 8–12 at%; Fe³⁺ is concentrated in exsolved clusters of Mg_{1+x}Fe_{2-x}O_{4-x/2}, while all remaining iron in fPer is in the ferrous, Fe²⁺, state;
- Iron contents in both Bridg and fPer increase with depth (pressure), reflecting the increasing Fe content in the lower part of the lower mantle;
- Al content in Bridg from the lower part of the lower mantle is at ~10–12 wt% Al₂O₃ (Table 2);
- Al in Bridg occurs mainly in the cation B site and partly in the cation A site, in both cases substituting for Si, Mg, and Fe with vacancy formation; and in the case of Al positioning in both B and A sites, a charge-balanced reaction.

These observations in natural samples cannot be simply explained by the dissolution of Al in Bridg and the spin transition of Fe²⁺ in fPer. The differences between observations in natural samples and experimental results should be taken into account in future calculations and experimental works.

ACKNOWLEDGMENTS

We thank W. Bassett and an anonymous reviewer for their careful, constructive reviews, which helped us to improve the manuscript. Particular thanks are also due to the Editor Fabrizio Nestola for his efficient handling of the manuscript.

REFERENCES CITED

- Akber-Knutson, S., and Bukowski, M.S.T. (2004) The energetics of aluminum solubility into MgSiO₃ perovskite at lower mantle conditions. *Earth and Planetary Science Letters*, 220, 317–330, doi:10.1016/S0012-821X(04)00065-2.
- Andraut, D. (2001) Evaluation of (Mg,Fe) partitioning between silicate perovskite and magnesiowüstite up to 120 GPa and 2300 K. *Journal of Geophysical Research*, 106, 2079–2087.
- Andraut, D., Bolfan-Casanova, N., Bouhifd, M.A., Guignot, N., and Kawamoto, T. (2007) The role of Al-defects on the equation of state of Al-(Mg,Fe)SiO₃ perovskite. *Earth and Planetary Science Letters*, 263, 167–179, doi:10.1016/j.epsl.2007.08.012.
- Auzende, A.-L., Badro, J., Ryerson, F.J., Weber, P.K., Fallon, S.J., Addad, A., Siebert, J., and Fiquet, G. (2008) Element partitioning between magnesium silicate perovskite and ferropericlase: New insights into bulk lower-mantle geochemistry. *Earth and Planetary Science Letters*, 269, 164–174, doi:10.1016/j.epsl.2008.02.001.
- Badro, J., Fiquet, G., Guyot, F., Rueff, J.-P., Struzhkin, V.V., Vankó, G., and Monaco, G. (2003) Iron partitioning in Earth's mantle: Toward a deep lower mantle discontinuity. *Science*, 300, 789–791, doi:10.1126/science.1081311.
- Bower, D.J., Wicks, J.K., Gurnis, M., and Jackson, J.M. (2011) A geodynamic and mineral physics model of a solid-state ultralow-velocity zone. *Earth and Planetary Science Letters*, 303, 193–202, doi:10.1016/j.epsl.2010.12.035.
- Cammarano, F., Marquardt, H., Speziale, S., and Tackley, P.J. (2010) Role of iron-spin transition in ferropericlase on seismic interpretation: A broad thermochemical transition in the mid mantle? *Geophysical Research Letters*, 37, L03308, doi:10.1029/2009GL041583.
- Davies, R.M., Griffin, W.L., O'Reilly, S.Y., and Doyle, B.J. (2004) Mineral inclusions and geochemical characteristics of microdiamonds from the DO27, A154, A21, A418, DO18, DD17 and Ranch Lake kimberlites at Lac de Gras, Slave Craton, Canada. *Lithos*, 77, 39–55, doi:10.1016/j.lithos.2004.04.016.

- Dziewonski, A.M., and Anderson, D.L. (1981) Preliminary reference Earth model. *Physics of the Earth and Planetary Interiors*, 25, 297–356.
- Frost, D.J., and McCammon, C.A. (2008) The redox state of Earth's mantle. *Annual Review of Earth and Planetary Sciences*, 36, 389–420, doi:10.1146/annurev.earth.36.031207.124322.
- Frost, D.J., Liebske, C., Langenhorst, F., McCammon, C.A., Trønnes, R.G., and Rubie D.C. (2004) Experimental evidence for the existence of iron-rich metal in the Earth's lower mantle. *Nature*, 428, 409–412, doi:10.1038/nature02413.
- Garnero, E., and McNamara, A. (2008) Structure and dynamics of Earth's lower mantle. *Science*, 320, 626–628, doi:10.1126/science.1148028.
- Guyot, F., Madon, M., and Poirier, J.-P. (1988) X-ray microanalysis of high pressure/high temperature phases synthesized from natural olivine in the diamond–anvil cell. *Earth and Planetary Science Letters*, 90, 52–64, doi:10.1016/0012-821X(88)90110-0.
- Harte, B., Harris, J.W., Hutchison, M.T., Watt, G.R., and Wilding, M.C. (1999) Lower mantle mineral associations in diamonds from Sao Luiz, Brazil. *Geochemical Society, Special Publication No. 6*, 125–153.
- Hayman, P.C., Kopylova, M.G., and Kaminsky, F.V. (2005) Lower mantle diamonds from Rio Soriso (Juina, Brazil). *Contributions to Mineralogy and Petrology*, 149, 430–445, doi:10.1007/s00410-005-0657-8.
- Hsu, H., Yu, Y.G., and Wentzcovitch, R.M. (2012) Spin crossover of iron in aluminous MgSiO₃ perovskite and post-perovskite. *Earth and Planetary Science Letters*, 294, 19–26, doi:10.1016/j.epsl.2010.02.031.
- Hutchison, M.T. (1997) Constitution of the deep transition zone and lower mantle shown by diamonds and their inclusions. Unpublished Ph.D. thesis, 306 pp. University of Edinburgh, U.K.
- Irfune, T. (1994) Absence of an aluminous phase in the upper part of the Earth's lower mantle. *Nature*, 370, 131–133, doi:10.1038/370131a0.
- Irfune, T., and Tsuchiya, T. (2007) Mineralogy of the Earth—Phase transitions and mineralogy of the lower mantle. *Treatise on Geophysics*, 2, 33–62.
- Irfune T., Shimmei T., McCammon C.A., Miyajima N., Rubie D.C., and Frost D.J. (2010) Iron partitioning and density changes of pyrolite in Earth's lower mantle. *Science*, 327, 193–195, doi:10.1126/science.1181443.
- Kaminsky, F.V. (2012) Mineralogy of the lower mantle: A review of 'super-deep' mineral inclusions in diamond. *Earth-Science Reviews*, 110, 127–147, doi:10.1016/j.earscirev.2011.10.005.
- Kaminsky, F.V., Ryabchikov, I.D., McCammon, C., Longo, M., Abakumov, A.M., Turner, S., and Heidari, H. (2015a) Oxidation potential in the Earth's lower mantle as recorded from ferropericlase inclusions in diamond. *Earth and Planetary Science Letters*, 417, 49–56, doi:10.1016/j.epsl.2015.02.029.
- Kaminsky, F.V., Wirth, R., and Schreiber, A. (2015b) A microinclusion of lower-mantle rock and some other lower-mantle inclusions in diamond. *Canadian Mineralogist*, 53, 83–104, doi:10.3749/canmin.1400070.
- Katsura, T., and Ito, E. (1996) Determination of Fe–Mg partitioning between perovskite and magnesio-wüstite. *Geophysical Research Letters*, 23, 2005–2008.
- Kennett, B., Engdahl, E., and Buland, R. (1995) Constraints on seismic velocities in the Earth from traveltimes. *Geophysical Journal International*, 122, 108–124, doi:10.1111/j.1365-246X.1995.tb03540.x.
- Kesson, S.E., and Fitz Gerald, J.D. (1991) Partitioning of MgO, FeO, NiO, MnO and Cr₂O₃ between magnesian silicate perovskite and magnesio-wüstite: implications for the origin of inclusions in diamond and the composition of the lower mantle. *Earth and Planetary Science Letters*, 111, 229–240.
- Kesson S.E., Fitz Gerald, J.D., and Shelley, J.M. (1998) Mineralogy and dynamics of a pyrolite lower mantle. *Nature*, 393, 252–255, doi:10.1016/0012-821X(92)90181-T.
- Kesson, S.E., Fitz Gerald, J.D., O'Neill, H.St.C., and Shelley, J.M.G. (2002) Partitioning of iron between magnesian silicate perovskite and magnesio-wüstite at about 1 Mbar. *Physics of the Earth and Planetary Interiors* 131, 295–310, doi:10.1016/S0031-9201(02)00063-8.
- Kobayashi, Y., Kondo, T., Ohtani, E., Hirao, N., Miyajima, N., Yagi, T., Nagase, T., and Kikegawa, T. (2005) Fe–Mg partitioning between (Mg, Fe)SiO₃ post-perovskite, perovskite, and magnesio-wüstite in the Earth's lower mantle. *Geophysical Research Letters*, 32, L19301, doi:10.1029/2005GL023257.
- Lee, K.K.M., O'Neill, B., Panero, W.R., Shim, S.H., Benedetti, L.R., and Jeanloz, R. (2004) Equations of state of the high-pressure phases of a natural peridotite and implications for the Earth's lower mantle. *Earth and Planetary Science Letters* 223 (3–4), 381–393, doi:10.1016/j.epsl.2004.04.033.
- Lin, J.F., Vankó, G., Jacobsen, S.D., Iota, V., Struzhkin, V.V., Prakapenka, V.B., Kuznetsov, A., and Yoo, C.-S. (2007) Spin transition zone in Earth's lower mantle. *Science*, 317, 1740–1743, doi:10.1126/science.1144997.
- Lin, J.F., Speciale, S., Mao, Z., and Marquardt, H. (2013) Effects of the electronic spin transitions of iron in lower mantle minerals: implications for deep mantle geophysics and geochemistry. *Reviews in Geophysics*, 51, 244–275, doi:10.1029/2012RG000210.
- Liu, Z., Irfune, T., Nishi, M., Tange, Y., Arimoto, T., and Shimmei, T. (2016) Phase relations in the system MgSiO₃–Al₂O₃ up to 52 GPa and 2000 K. *Physics of the Earth and Planetary Interiors*, 257, 18–27, doi:10.1016/j.pepi.2016.05.006.
- Mao, Z., Lin, J.F., Jacobs, C., Watson, H., Xiao, Y., Chow, P., Alp, E.E., and Prakapenka, V.B. (2010) Electronic spin and valence states of Fe in CaIrO₃-type post-perovskite in the Earth's lowermost mantle. *Geophysical Research Letters*, 37, L22304.
- McCammon, C., Hutchison, M.T., and Harris J.W. (1997) Ferric iron content of mineral inclusions in diamonds from São Luiz: A view into the lower mantle. *Science*, 278, 434–436, doi:10.1126/science.278.5337.434.
- McDonough, W.F., and Sun, S.-S. (1995) The composition of the Earth. *Chemical Geology*, 120, 223–253, doi:10.1016/0009-2541(94)00140-4.
- Muir, J.M.R., and Brodholt, J.P. (2016) Ferrous iron partitioning in the lower mantle. *Physics of the Earth and Planetary Interiors*, 257, 12–17, doi:10.1016/j.pepi.2016.05.008.
- Murakami, M., Hirose, K., Sata, N., and Ohishi, Y. (2005) Post-perovskite phase transition and mineral chemistry in the pyrolitic lowermost mantle. *Geophysical Research Letters*, 32, L03304, doi:10.1029/2004GL021956.
- Nestola, F., Burnham, A., Peruzzo, L., Tauro, L., Alvaro, M., Walter, M.J., and Gunther, M. (2015) Jeffbenite, IMA 2014-097. *CNMNC Newsletter No. 24*, April 2015, page 250. *Mineralogical Magazine*, 79, 247–251, doi:10.1180/minmag.2016.080.059.
- Nestola, F., Cerantola, V., Milani, S., Anzolini, C., McCammon, C., Novella, D., Kuznetsov, I., Chumakov, A., Rüfner, R., and Harris, J.W. (2016) Synchrotron Mössbauer Source technique for in situ measurement of iron-bearing inclusions in natural diamonds. *Lithos*, doi:10.1016/j.lithos.2016.06.016.
- Richmond, N.C., and Brodholt, J.P. (1998) Calculated role of aluminum in the incorporation of ferric iron into magnesium silicate perovskite. *American Mineralogist*, 83, 947–951.
- Ryabchikov, I.D., and Kaminsky, F.V. (2013) Oxygen potential of diamond formation in the lower mantle. *Geology of Ore Deposits*, 55, 1–12, doi:10.1134/S1075701513010066.
- Sakai, T., Ohtani, E., Terasaki, H., Sawada, N., Kobayashi, Y., Miyahara, M., Nishijima, M., Hirao, N., Ohishi, Y., and Kikegawa, T. (2009) Fe–Mg partitioning between perovskite and ferropericlase in the lower mantle. *American Mineralogist* 94, 921–925, doi:10.2138/am.2009.3123.
- Sinmyo, R., and Hirose, K. (2013) Iron partitioning in pyrolitic lower mantle. *Physics and Chemistry of Minerals*, 40, 107–113, doi:10.1007/s00269-012-0551-7.
- Speziale, S., Milner, A., Lee, V.E., Clark, S.M., Pasternak, M.P., and Jeanloz, R. (2005) Iron spin transition in Earth's mantle. *Proceedings of the National Academy of Sciences*, 102, 17918–17922, doi:10.1073/pnas.0508919102.
- Stachel, T., Harris, J.W., Brey, G.P., and Joswig, W. (2000) Kankan diamonds (Guinea) II: lower mantle inclusion parageneses. *Contributions to Mineralogy and Petrology* 140, 16–27, doi:10.1007/s004100000174.
- Tange, Y., Takahashi, E., Nishihara, Y., Funakoshi, K., and Sata, N. (2009) Phase relations in the system MgO–FeO–SiO₂ to 50 GPa and 2000° C: An application of experimental techniques using multi-anvil apparatus with sintered diamond anvils. *Journal of Geophysical Research*, 114, B02214.
- Tappert, R., Foden, J., Stachel, T., Muehlenbachs, K., Tappert, M., and Wills, K. (2009) Deep mantle diamonds from South Australia: A record of Pacific subduction at the Gondwanan margin. *Geology*, 37, 43–46, doi:10.1130/G25055A.1.
- Thomson, A.R., Walter, M.J., Kohn, S.C., and Brooker, R.A. (2016) Slab melting as a barrier to deep carbon subduction. *Nature*, 529, 76–79.
- Tschauner, O., Ma, C., Beckett, J.R., Prescher, C., Prakapenka, V.B., and Rossman, G.R. (2014) Discovery of bridgmanite, the most abundant mineral in Earth, in a shocked meteorite. *Science*, 346, 1100–1102, doi:10.1126/science.1259369.
- Tsuchiya, T., Wentzcovitch, R.M., da Silva, C.R.S., and de Gironcoli, S. (2006) Spin transition in magnesio-wüstite in Earth's lower mantle. *Physical Review Letters* 96, 198501, doi:10.1103/PhysRevLett.96.198501.
- Vilella, K., Shim, S.-H., Farnetani, C.G., and Badro, J. (2015) Spin state transition and partitioning of iron: Effects on mantle dynamics. *Earth and Planetary Science Letters*, 417, 57–66, doi:10.1016/j.epsl.2015.02.009.
- Wood, B.J. (2000) Phase transformations and partitioning relations in peridotite under lower mantle conditions. *Earth and Planetary Science Letters*, 174, 341–354.
- Wood, B.J., and Rubie, D.C. (1996) The effect of alumina on phase transformations at the 660-kilometer discontinuity from Fe–Mg partitioning experiments. *Science*, 273, 1522–1524.
- Wu, Z., and Wentzcovitch, R.M. (2014) Spin crossover in ferropericlase and velocity heterogeneities in the lower mantle. *Proceedings of the National Academy of Sciences*, 111, 10,468–10,472, doi:10.1073/pnas.1322427111.
- Xu, S., Lin, J.-F., and Morgan, D. (2017) Iron Speciation Induced Chemical and Seismic Heterogeneities in the Lower Mantle. *Journal of Geophysical Research: Solid Earth*, 122, B51982, doi:10.1002/2016JB013543.
- Yang, J., Tong, X., Lin, J.F., Tomioka, N., Okuchi, T., and Prakapenka, V.B. (2015) Elasticity of ferropericlase across the spin crossover in the Earth's lower mantle. *Scientific Reports*, 5, 17188, doi:10.1038/srep17188.
- Zhang, L., Meng, Y., Yang, W., Wang, L., Mao, W.L., Zeng, Q.S., Jeong, J.S., Wagner, A.J., Mkhoyan, K.A., Liu, W., Xu, R., and Mao, H.K. (2014) Disproportionation of (Mg,Fe)SiO₃ perovskite in Earth's deep lower mantle. *Science*, 344, 879–882.
- Zedgenizov D.A., Kagi H., Shatsky V.S., and Ragozin A.L. (2014) Local variations of carbon isotope composition in diamonds from Sao-Luis (Brazil): evidence for heterogenous carbon reservoir in sublithospheric mantle. *Chemical Geology*, 240, 114–124, doi:10.1016/j.chemgeo.2013.10.033.

MANUSCRIPT RECEIVED SEPTEMBER 6, 2016

MANUSCRIPT ACCEPTED NOVEMBER 21, 2016

MANUSCRIPT HANDLED BY FABRIZIO NESTOLA